Sustainable Energy & Fuels

Interdisciplinary research for the development of sustainable energy technologies

Accepted Manuscript

This article can be cited before page numbers have been issued, to do this please use: E. Herrero and A. Ferre-Vilaplana, *Sustainable Energy Fuels*, 2019, DOI: 10.1039/C9SE00262F.

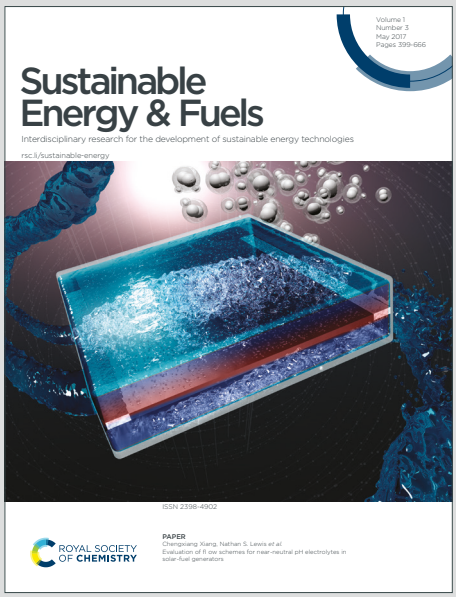

View Article Online
DOI: 10.1039/C9SE00262F

ARTICLE

Why nitrogen favors oxygen reduction on graphitic materials

Adolfo Ferre-Vilaplana[a]* and Enrique Herrero[b]*

Received 00th January 20xx,
Accepted 00th January 20xx

DOI: 10.1039/x0xx00000x

Nitrogen-doped graphitic materials as promising catalysts for the oxygen reduction reaction in fuel-cells have been mainly investigated under the graphitic versus pyridinic nitrogen-dopant dichotomy approach. However, we show here that active sites, reaction mechanism, selectivity and even the origin of each behavior can be better understood when the stability of the possible active site and the eventual contribution of charge from the surface are considered separately. The roles in the reaction played by specific nitrogen-dopants, the hydrogenation of pyridinic nitrogen-dopants and the solvation effect are all clarified. The investigated activity is much more linked to the edges, where certain carbon atoms are sufficiently unstable or can be destabilized by means of adjacent nitrogen-dopants, and where reaction intermediates can be better relaxed, than to the presence of specific nitrogen-dopants. Unfortunately, high overpotentials and the undesired production of hydrogen peroxide appear unavoidable in the oxygen reduction to water on these materials.

Introduction

The controlled oxidation of fuels in electrochemical cells could give rise to a more efficient and cleaner energy conversion technology than combustion engines. As a counterpart, both the fuel oxidation reaction on anodes and the oxygen reduction reaction (ORR) on cathodes, inside the fuel-cells, require of suitable catalysts.[1–4] Molecular oxygen on cathodes can be partially reduced to hydrogen peroxide and completely to water. The production of hydrogen peroxide decreases the fuel-cell performance and can degrade the device,[5] but it can be also the target of synthesis cells.[6]

Metal-free nitrogen-doped graphitic materials (NGs) exhibit activity towards the ORR,[7–9] though the active sites and the mechanisms have not been yet completely understood[10–28] preventing optimizations. ORR active sites on NGs have been mainly investigated under the graphitic versus pyridinic nitrogen-dopant dichotomy approach,[15–17] giving rise to one of the most controverted topics regarding these materials. Additionally, recent results suggest that XPS peaks attributed to pyrrolic nitrogen-dopants would be actually linked to hydrogenated-pyridinic nitrogen-dopants.[29,30] Using highly oriented pyrolytic graphite with well-defined π-conjugation and well-controlled nitrogen-doping, it has been recently concluded that ORR activity on NGs should be attributed to the presence of pyridinic nitrogen-dopants,[16] reinforcing previous results.[8,18–20] However, we will show that such a conclusion is not accurate enough. It has been suggested that graphitic nitrogen-dopants also play a role in the mechanism,[15,21,31] and we will demonstrate that basal plane versus edge and even type of edge (armchair versus zigzag) are also essential dichotomies to completely understanding ORR on NGs.

ORR activity on NGs is frequently attributed to the positive charge originated on carbon atoms adjacent to nitrogen.[7,8,32] It has been also attributed to spin-polarization effects on that carbon atoms.[14,33] However, these effects can be considered neither the primary nor the ultimate mechanisms but only manifestations of the true mechanisms. The electronic structure of the surface before activation can influence the kinetics. But the true relevance of a given site, regarding a given multi-step reaction, is ultimately dictated by the thermodynamic profile of the whole of the reaction on the site. On the other hand, ORR activity has been linked to Lewis basicity on these materials.[16]

It has been pointed out that configurations of nitrogen-dopants in clusters would be high energy defects.[22,34] However, we found that important effects influencing the ORR on NGs are not captured when a single nitrogen dopant is included in the model.[6,35,36] Moreover, it has been shown that the hydrogenation of pyridinic nitrogen-dopants also plays a role in the mechanism.[6,17,36–38] Finally, the associative mechanism of the reaction has been emphasized as the relevant mechanism on these materials.[14] Assuming these insights, the complete ORR reaction on a broad set of unclustered nitrogen-dopants configurations is here theoretically investigated at the free energy level using DFT. From these results, the active sites, the reaction mechanism and its selectivity, the roles played by specific nitrogen-dopants and by the hydrogenation of pyridinic nitrogen-dopants, the solvation effect and even the origin of each behavior are all clarified. It is found that ORR activity on NGs is much more linked to the edges than to the presence of specific

[a] Instituto Tecnológico de Informática, Ciudad Politécnica de la Innovación, Camino de Vera s/n, E-46022 Valencia, Spain, and Departamento de Sistemas Informáticos y Computación, Escuela Politécnica Superior de Alcoy, Universidad Politécnica de Valencia, Plaza Ferrándiz y Carbonell s/n, E-03801 Alcoy, Spain.
[b] Instituto de Electroquímica, Universidad de Alicante, Apdo. 99, E-03080 Alicante, Spain

Electronic Supplementary Information (ESI) available: See
DOI: 10.1039/x0xx00000x

nitrogen-dopants. At these regions, certain carbon atoms are sufficiently unstable, or can be destabilized by means of adjacent nitrogen-dopants, and reaction intermediates can be better relaxed. The proposed mechanisms involve a local component, in the form of a sufficiently unstable carbon atom, and a global component, in the form of available charge. Carbon atoms can be destabilized as a local effect of both graphitic and hydrogenated-pyridinic nitrogen-dopants (depending on the region of the material), and charge can be globally contributed from both graphitic and hydrogenated-pyridinic nitrogen-dopants. Both effects would be in the core of the ORR activity, selectivity and Lewis basicity of these materials. Unfortunately, high overpotentials and the undesired production of hydrogen peroxide would be unavoidable in the oxygen reduction to water on NGs.

Methods

Using numerical basis sets[39] under the PBE functional,[40] periodic DFT calculations at neutral charge were performed running Dmol^3.[41] All the electrons were explicitly included in the calculations under a spin unrestricted approach. Explicit water molecules and the COSMO[42] continuum solvation model were used as solvation effect treatment. Dispersion forces were taken into account by the Tkatchenko and Scheffler method.[43] Non-zero dipole moments in the supercells were cancelled by means of external fields.[44] Free energy profiles were obtained by correcting DFT total energies for zero point vibrational energies and entropies. Potential effects were incorporated into the free-energy profiles by means of the computational hydrogen electrode formalism.[45] Additional details are provided in the Electronic Supplementary Information.

Results and discussion

Energy profiles.

The complete associative mechanism of the ORR can be schematized as:

$$O_2 \rightarrow OO_{ads} \rightarrow OOH_{ads} \rightarrow O_{ads} + H_2O \rightarrow OH_{ads} + H_2O \rightarrow 2H_2O \quad (1)$$
$$\downarrow$$
$$H_2O_2$$

Therefore, the free-energy profiles for the ORR on the NG configurations displayed in Figure 1 were estimated, using DFT, considering the intermediate states: (1) free O_2, (2) OO_{ads}, (3) OOH_{ads}, (4) O_{ads} and (5) OH_{ads}. Each energy value was obtained as the ΔG of the full cell reaction for the conversion of the corresponding intermediate into the surface (S) plus two water molecules. Thus, the calculated ΔG values are those of to the reactions:

$$S + O_2 + 2H_2 \rightarrow S + 2H_2O \quad (2)$$

$$OO_{ads} + 2H_2 \rightarrow S + 2H_2O \quad (3)$$

$$OOH_{ads} + \frac{3}{2}H_2 \rightarrow S + 2H_2O \quad (4)$$

$$O_{ads} + H_2 + H_2O \rightarrow S + 2H_2O \quad (5)$$

$$OH + \frac{1}{2}H_2 + H_2O \rightarrow S + 2H_2O \quad (6)$$

Each NG configuration is identified by a capital letter (G, Z or A) followed by two hyphen-separated symbols plus, eventually, the asterisk symbol. The capital letter identifies the type of configuration: G for graphene, Z for zigzag and A for armchair nanoribbons. The first of the two hyphen-separated symbols codify the site of a substitutional nitrogen-dopant (the local one), using 0 when missing. The second one codifies the carbon atom tested as the active site. Finally, an asterisk is added only when an additional substitutional nitrogen-dopant (the remote one) is introduced in the model (see Figure 1). So, the notation Z1-2* represents a graphitic material with abundant zigzag edges, modeled by the periodic unit cell displayed in Figure 1C, in which a substitutional nitrogen-dopant is introduced at the site identified as 1 and an additional one in the site identified by the asterisk symbol, and where the carbon atom identified as 2 is tested as the active site.

Table 1 summarizes the ORR free-energy profiles for the most relevant configurations, i.e., those with an asterisk, because in real materials there will be always additional nitrogen-dopants along with a given local one. The consideration of variations on these models allows concluding that the effect of the remote nitrogen-dopant is largely independent on the distance, the exact position and the type of nitrogen (graphitic or hydrogenated-pyridinic). The profiles corresponding to configurations without the asterisk are also included as Table S1 in the Electronic Supplementary Information for comparison.

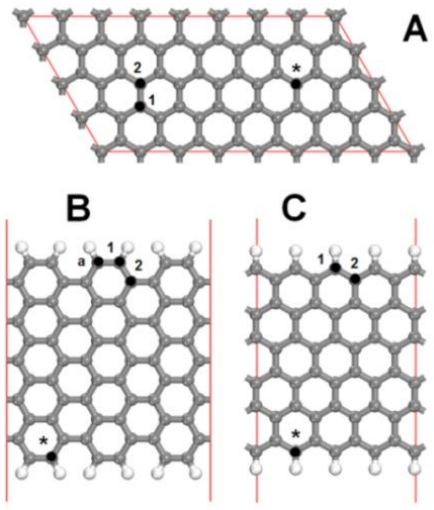

Figure 1. Unit cells and sites of the periodic models used to represent different materials: A) graphene, B) armchair and C) zigzag nanoribbons. Numbers identify sites tested both as hypothetical active carbon atom and as substitutional nitrogen-dopant. The "a" letter identifies an additional carbon atom tested as the possible active site. When additional nitrogen-dopants were included in the models, they were located in the asterisk-marked sites.

View Article Online
DOI: 10.1039/C9SE00262F

Table 1. Free-energy profiles in eV for the complete ORR reaction on different nitrogen-doped graphitic configurations.

Reactions	Configurations										
	G0-2*	G1-2*	Z0-1*	Z0-2*	Z1-2*	Z2-1*	A0-1*	A0-2*	A1-a*	A1-2*	A2-1*
OO (1)	-4.93	-4.93	-4.93	-4.93	-4.93	-4.93	-4.93	-4.93	-4.93	-4.93	-4.93
OO_{ads} (2)	-	-5.27	-4.97	-	-	-4.76	-	-	-4.45	-5.03	-4.98
OOH_{ads} (3) (stability)	-5.27	-4.64	-3.95 (0.36)	-	-5.57	-4.18 (0.33)	-4.98	-	-3.87 (0.13)	-4.72	-4.22
O_{ads} (4)	-3.32	-1.79	-2.09	-	-	-1.05	-	-	-1.18	-1.72	-1.43
OH_{ads} (5)	-2.07	-1.36	-0.55	-2.55	-2.35	-0.72	-1.76	-1.97	-0.54	-1.43	-0.98

The energy profiles G0-2, Z0-1, Z0-2, A0-1 and A0-2 (Table S1) suggest that, in the total absence of nitrogen (and other dopants and defects), neither on the basal plane nor at the edges graphitic materials can activate molecular oxygen through the OO_{ads} intermediate, though the Z0-1 configuration would be very close to that. Moreover, with the only exception of the Z0-1 configuration, not even OOH_{ads} would be favorable enough at low overpotentials on these configurations. By contrast, the profiles G1-2*, Z0-1*, Z2-1*, A1-a*, A1-2* and A2-1* (Table 1) provide evidence that, in the presence of nitrogen, the ORR can be favored on specific NG configurations, sites and conditions.

The potential-dependent energy profiles for the most relevant configurations at three different potentials are displayed in Figure 2. At E=0 V, these profiles are always downhill (within the error of the calculations) for all the at edge configurations having a remote nitrogen. Thus, all these configurations would be able to activate oxygen through the OO_{ads} intermediate and drive the full ORR to water at this electrode potential, though it does not imply complete selectivity. The OO_{ads} formation on the G1-2* configuration is unfavorable by ca. 0.34 eV, though OOH_{ads} could be also formed by a concerted proton-electron transfer from solution,[46,47] a process that would be favorable in this case. Finally, the OO_{ads} formation on the Z0-1 configuration is unfavorable by only ca. 0.23 eV. This small value, surmountable with thermal energy, implies that the Z0-1 configuration would be also active for the ORR, given that the rest of the steps would be straightforward. This last observation would explain the increase of the ORR activity on HOPG materials as the number of edges increase,[48] linking the activity to the presence of zigzag edges.

As the electrode potential increases, the ORR becomes progressively less favorable. At around E=0.60 V, only the A1-a* configuration maintains all the reaction steps downhill, with the intermediate states O_{ads} and OH_{ads} in virtual equilibrium (within the errors of the calculation) with H_2O. This is moreover the most favorable configuration for activation. Therefore, the complete ORR to water on NGs would be optimally favored at armchair edges below 0.60 V, being the reaction deactivated on zigzag edges at lower potentials. The value is close to the experimental onset value 0.67 V.[48] This configuration has been also pointed out from experiments.[20]

Finally, at *E*=1.23 V (the thermodynamic equilibrium potential for the ORR), the limiting steps in the reaction can be identified. For optimal performance (where the reaction would take place without significant overpotentials), all the intermediate energy levels (OOH_{ads}, O_{ads} and OH_{ads}) at this potential should have been the same and equal to that of

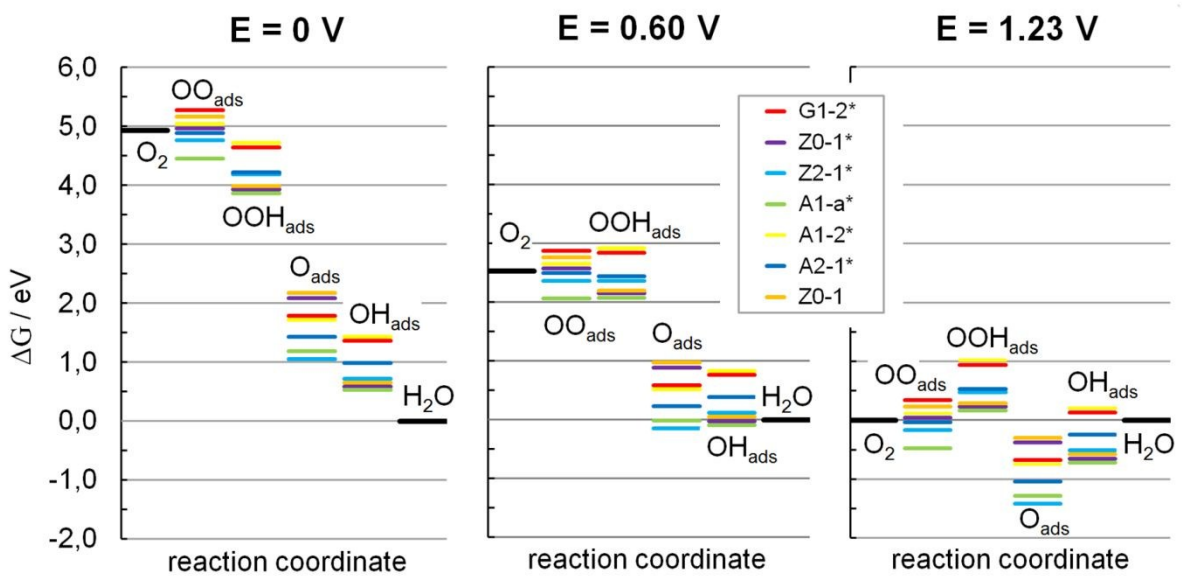

Figure 2. Free energy profiles for the ORR reaction on different nitrogen-doped graphitic configurations at different electrode potentials (vs. RHE).

reactants and products. However, OOH_{ads} formation for the most active configuration toward the complete reduction to water (A1-a*) is uphill by 0.17 eV, whereas O_{ads} and OH_{ads} are more stable than water by -1.29 and -0.69 eV, respectively. Thus, the most unfavorable steps for A1-a* are the OH_{ads} and O_{ads} removal. By contrast, the OOH_{ads} formation on the G1-2* configuration is unfavorable by 0.94 eV, being the molecular oxygen activation the most difficult step in this case.

Scaling laws

To optimize the catalyst, the OH_{ads} on the A1-a* configuration could be weakened. Alternatively, the OOH_{ads} on the G1-2* configuration could be strengthened. However, it has been shown that the OOR intermediate energy levels on metals are strongly correlated.[45] To explore these correlations on NGs, the reductive desorption free-energies of the intermediates OO_{ads}, OOH_{ads}, and O_{ads} (eqs. (3) to (5)) are plotted vs. that of OH_{ads} (E_{OHads} eq.(6)) in Figure 3. Linear relationships were obtained for all the intermediates. Thus, is here demonstrated that the scale law principle operates also on graphitic materials, which has been already pointed out.[49] However, a singular difference between the OO_{ads} and O_{ads} behavior with respect to OOH_{ads} on NGs deserves to be highlighted. Two different fittings for each one of the OO_{ads} and O_{ads} intermediates, depending on the presence or absence of remote nitrogen in the model, were required, implying that the remote nitrogen has a significant effect on the stabilization of these intermediates. By contrast, a single linear relationship allowed the perfect fitting of the OOH_{ads} for all the configurations.

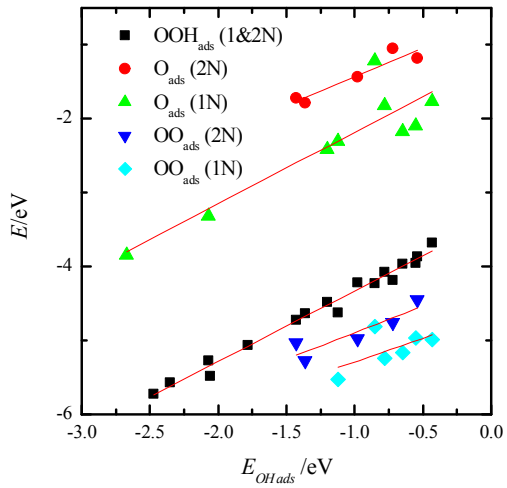

Figure 3. Free energy for the reductive desorption of OO_{ads}, OOH_{ads} and O_{ads} vs. that of OH_{ads} depending on the total number of nitrogen atoms in the lattice (1N or 2N).

Overpotentials

Considering the formation of OOH_{ads}, reduction of O_{ads} to OH_{ads} and desorption of OH_{ads} to form water as the potential limiting steps of the reaction, the performance of the best conceivable unclustered NG catalyst can be estimated assuming the scale laws displayed in Figure 3. The electrode potential as a function of the E_{OHads} for each intermediate step is plotted in Figure 4. The intermediate reaction having the lower potential is the limiting step for the whole of the ORR. Therefore, a truncated volcano curve for the effective electrode potential is obtained as a function of E_{OHads}. For small energy values of the OH_{ad} to water reaction, this is the limiting step. For large energy values for this reaction, the limiting step is the formation of OOH_{ads}. For intermediate values (-1.15< E_{OHads} <0.6 eV), the O_{ads} reduction to OH_{ads} is the limiting step. Thus, the truncated volcano curve points to a best performing value for E_{OHads} close to -0.6 eV, which imply high overpotentials. To break the scaling laws giving rise to high overpotentials, a second active site could be required.[50]

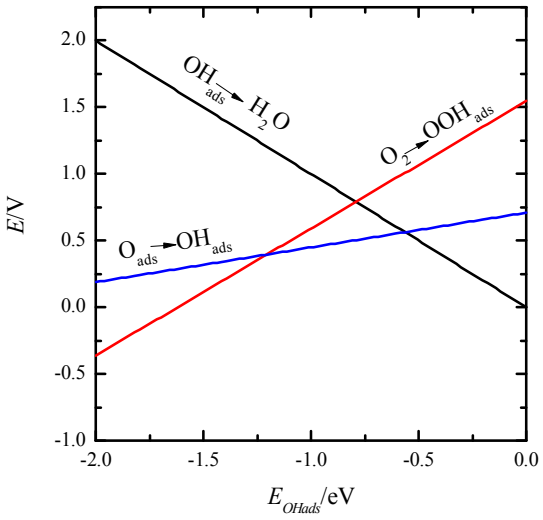

Figure 4. Energy for the different steps in the ORR as a function of E_{OH}, showing a truncated volcano curve.

Selectivity

The molecular oxygen reduction to hydrogen peroxide is thermodynamically possible for potentials below the standard redox potential of this reaction (0.69 V). The ORR to H_2O_2 free-energy profiles for the investigated NG configurations, according to the equations:

$$S + O_2 + H_2 \rightarrow S + H_2O_2 \quad (7)$$

$$OO_{ads} + H_2 \rightarrow S + H_2O_2 \quad (8)$$

$$OOH_{ads} + \frac{1}{2}H_2 \rightarrow S + H_2O_2 \quad (9)$$

are summarized for E=0 V in table S2 and displayed for E=0.65 V in Figure 5. All energy steps are very small, indicating that hydrogen peroxide can be always unavoidably produced when molecular oxygen is reduced to water on these materials, which is consistent with previous results.[6,15,21,51,52]

View Article Online
DOI: 10.1039/C9SE00262F

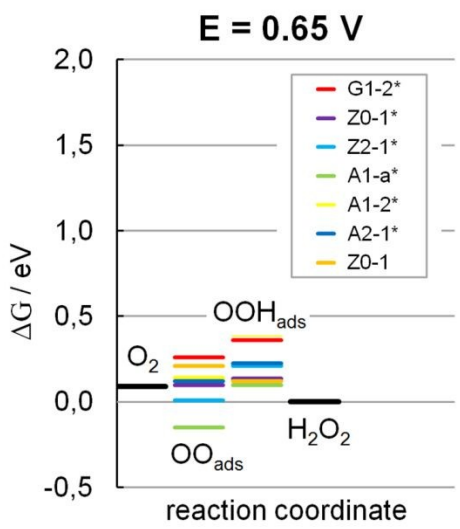

Figure 5. Free energy profiles for the ORR to H_2O_2 reaction at 0.65 V (vs. RHE).

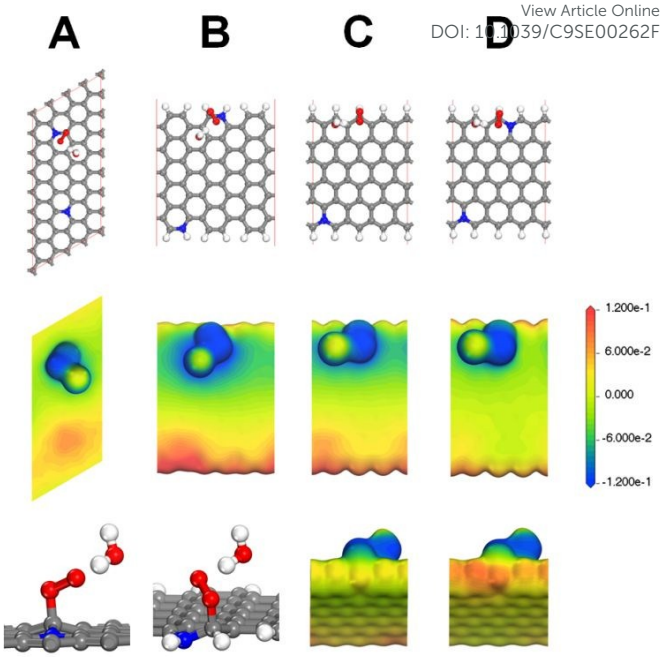

Figure 6. Monodentate associative chemisorbed states of molecular oxygen on different unclustered nitrogen-doped graphitic configurations. For each configuration, the nitrogen layout, the electrostatic potential [Ha per e] mapped on the density isosurface ρ=0.01 e A^{-3} and a significant detail are displayed.

Primary mechanisms

To associatively activate oxygen on NGs, the active carbon atom would have to bond the proximal oxygen atom of the molecule. The mechanism would involve the surface restructuration, the oxygen double bond degradation to single bond and the spin-polarized charge location at the distal oxygen. In the presence of available charge, additional charge could be paired at the distal oxygen. Though, in doing so, net charge would be accumulated at this atom. However, under solvation conditions, charge localized at the distal oxygen could be stabilized by the solvation effect. Thus, to associatively activate oxygen on NGs, relatively unstable carbon atoms and available charge would be required, being the solvation effect essential.

Conditions under which the described mechanism could become to operate have been previously identified. [35] It was found that graphitic nitrogen-dopants, from the basal plane of unclustered NGs, can contribute charge to even large distance (Figure 6A), which is consistent with the observation that graphitic nitrogen-dopants delocalize charge on graphene.[53] Moreover, it was found that unclustered graphitic nitrogen-dopants at the basal plane destabilize their adjacent carbon atoms, and that the net charge located at the distal oxygen of an adsorbed oxygen molecule can be, in fact, stabilized by the solvation effect.[35] Alternatively, ORR on NGs has been also explained from superoxide.[54] However, in any case, it has been here shown that graphitic nitrogen-dopants at the basal plane cannot sufficiently destabilize their adjacent carbon atoms to drive ORR under favorable conditions, which is consistent with previous results.[16]

Moreover, from Figure 6B-C can be concluded that, also from the edges, both graphitic and hydrogenated-pyridinic nitrogen-dopants can contribute charge to even large distance when they are not involved in the activation of an adjacent carbon atom. Additionally, when A0-a* and A0-1* vs. A1-a* and A2-1* energy profiles are compared (Table 1), it can be concluded that both graphitic and hydrogenated-pyridinic nitrogen-dopants destabilize certain adjacent carbon atoms at armchair edges, favoring their activation. Finally, the Z0-1* energy profile (Table 1) reveals that, in presence of available charge, carbon atoms at pristine zigzag edges are unstable enough as for activating oxygen, and the Z2-1* one (Table 1), that hydrogenated-pyridinic nitrogen-dopants cannot destabilize their adjacent carbon atoms at zigzag edges.

Unfortunately, the inherent capability of contributing charge from the surface, which favors the molecular oxygen activation on NGs, drives desorption of the undesired hydrogen peroxide anion. To this end, when Z0-1* and Z2-1* energy profiles are compared (Tables 1 and S1), with the aid of Figure 6C-D, it can be observed that, in the presence of adjacent nitrogen-dopants, the required charge for the activation at zigzag edges is more favorably contributed from the local nitrogen-dopant than from the remote one. This is so because the activating carbon atom is already unstable enough on pristine zigzag edges. The local contribution of charge locally polarizes the chemisorbed complex, stabilizing the hydrogen peroxide anion, though only until 0.33 eV.

Ultimate mechanisms

In brief, nitrogen favors the ORR on NGs because both graphitic and hydrogenated-pyridinic nitrogen-dopants can

both destabilize certain adjacent carbon atoms and contribute with charge, but why? Graphitic nitrogen-dopants can contribute with charge because they delocalized charge on the surface when they are not involved in the activation of an adjacent carbon atom. Regarding the ORR on NGs, the electron-accepting capability of nitrogen has been emphasized.[7] Also, the role of the graphitic nitrogen-dopants delocalizing charge on graphene has been pointed out.[53] The apparent contradiction can be conciliated. The over stabilization originated by the collective nature of the graphitic network, to which each carbon atom contribute with four electrons, would be drastically reduced if each graphitic nitrogen-dopant would contribute to the structure with only three electrons. This argument suggests that each graphitic-nitrogen dopant contributes to the surface with additional charge, involving its 2s electrons. First, the higher electronegativity and positive charge at the nucleus displace bonding charge toward the nitrogen atom (Figure 7A-C). Then, charge is partially delocalized from nitrogen to their adjacent carbon atoms, to compensate the previously displaced charge toward the nitrogen atom, and on the surface, avoiding the nitrogen atom itself (Figure 7D-F). So, part of the delocalized charge on the surface can be easily contributed to even large distance. This mechanism would explain why graphitic nitrogen-dopants favor the ORR on NGs having an effect on the limiting current[15] and on the current density.[21]

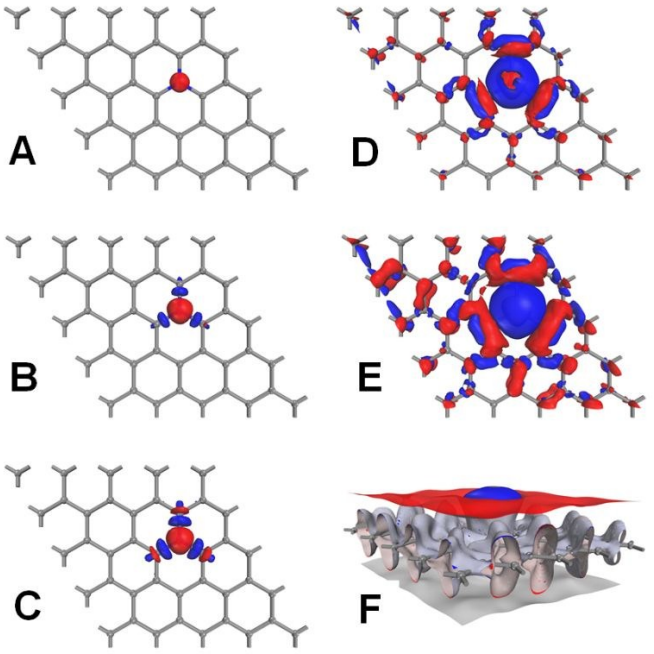

Figure 7. Electron density difference isosurfaces between graphene models with and without a graphitic nitrogen-dopant at A) $\pm5\times10^{-1}$ B) $\pm1\times10^{-1}$ C) $\pm5\times10^{-2}$ D) $\pm1\times10^{-2}$ E) $\pm5\times10^{-3}$ and F) $\pm1\times10^{-5}$ e Å^{-3}. The red color visualizes regions of charge concentration, meanwhile the blue color represents regions of charge depletion.

Hydrogenated-pyridinic nitrogen-dopants can contribute charge because, when they are not involved in the activation of an adjacent carbon atom, they adopt a sp^2-hybridized configuration, which gives rise to delocalized charge on the surface. Before molecular oxygen activation, and after the hydrogenation process, hydrogenated-pyridinic nitrogen-dopants remain coplanar to the surface, which is the signature of the sp^2 hybridization of orbitals. The structure can be then described as a proton, bonded to the lone pair exposed by the pyridinic nitrogen-dopant, plus a neutralizing electron, which is partially localized on the proton and partially delocalized on the surface. So, part of this delocalized charge can be easily contributed to even large distance. Note that the hydrogenation process is essential for pyridinic nitrogen to contribute charge.[36] This mechanism supports the observation that pyridinic nitrogen-dopants favor the ORR on NGs enhancing the current density.[21]

Both graphitic and hydrogenated-pyridinic nitrogen-dopants destabilize certain adjacent carbon atoms because they can exhibit a bimodal bonding behavior, minimizing the reorganization required to bind intermediates and maximizing the relaxation of the resulting chemisorbed states. Before molecular oxygen activation, both graphitic and hydrogenated pyridinic nitrogen-dopants lie coplanar to the surface, adopting sp^2 orbitals-hybridization. However, as can be observed in Figure 6A-B, after molecular oxygen activation, the nitrogen-dopant and the adjacent activated carbon atom tend to be displaced out of the plane in opposite directions. More precisely, each one of them tends to occupy the center of the tetrahedron defined by the atoms they are bonded to (for nitrogen, a vertex is missing). Therefore, being the tetrahedral disposition a signature of the sp^3 hybridization of orbitals, the activation implies the switching of the activated carbon atom from sp^2-hybridization to sp^3. This transition is favored, on certain nitrogen-doped graphitic configurations, when accompanied by the same kind of transition of an adjacent nitrogen atom. To activate oxygen, the electronic structure around the active carbon atom must be reorganized so that it can adopt the sp^3-hybridization. This reorganization destroys collective aromatic energy. Therefore, the smaller the reorganization to activate a carbon atom is required, the more unstable the carbon atom is. Nitrogen-dopants can destabilize carbon atoms because specific nitrogen-dopants can reduce the reorganization required to activate carbon atoms. The reorganization required to activate oxygen is relatively small at zigzag edges (Z0-1 and Z2-1), and it can be sufficiently reduced at armchair edges in the presence of adjacent graphitic and hydrogenated-pyridinic nitrogen-dopants (A2-1 and A1-a). On A1-a* (the most active configuration), the electronic structure reorganization required to bond oxygen is mainly limited to a single ring (inside the ring, both the active carbon and the adjacent nitrogen-dopant can switch from sp^2 to a sp^3). As a result, little aromaticity is destroyed, reason why the oxygen activation becomes favorable. By contrast, the reorganization required to activate oxygen cannot be sufficiently reduced neither in the presence of graphitic nitrogen-dopants at the basal plane nor on the carbon atoms adjacent to hydrogenated-pyridinic nitrogen-dopants at zigzag edges. On Z1-2*, the electronic structure reorganization required to bond oxygen would involve the whole edge, which would imply large aromaticity destruction, being thus unfavorable.

Moreover, when the sp^2 to sp^3 switching of the activated carbon atom is coordinately accompanied by the corresponding switching of an adjacent nitrogen atom, the resulting chemisorbed complexes that can be better relaxed. The described mechanism supports the observations, that molecular oxygen cannot be favorably activated in the basal plane,[16] and that ORR activity is favored by pyridinic-nitrogen dopants at the edges.[16,18–20]

Finally, both graphitic and hydrogenated-pyridinic nitrogen-dopants can exhibit bimodal bonding behavior (sp^2-sp^3) because switching is favored by the fact that their most favorable electronic configuration before activation (sp^2) is, somehow, suboptimal (they give rise to delocalized charge on the surface). When graphitic nitrogen-dopants switch from sp^2 before activation to sp^3 after activation, the charge delocalized before activation can be re-localized recovering energy. And, when hydrogenated pyridinic nitrogen-dopants switch from sp^2 before activation to sp^3 after activation, hydrogen can be covalently bonded to nitrogen diminishing the energy. Note that hydrogenation is essential for pyridinic nitrogen to adopt the described bimodal bonding behavior.

Conclusions

It has been shown that NGs cannot favorably drive the ORR in the basal plane and that in the presence of both graphitic and/or hydrogenated-pyridinic nitrogen dopants oxygen can be activated on certain carbon atoms at the edges of these materials. Thus, the investigated activity is much more linked to the edges, where certain carbon atoms are sufficiently unstable or can be destabilized by means of adjacent nitrogen-dopants, and where reaction intermediates can be better relaxed, than to the presence of specific nitrogen-dopants. Unfortunately, high overpotentials and the undesired production of hydrogen peroxide appear unavoidable to completely reduce oxygen to water on these materials. These results are consistent with, and provide reasoned explanations for, a broad set of experimental evidences, enabling to conciliate previous results. The here described mechanisms for the bimodal bonding behavior and charge contribution would be in the core explaining activity and selectivity of the ORR on NGs. Both graphitic and hydrogenated-pyridinic nitrogen-dopants can play these roles. Our results can contribute to the better understanding and future development of nitrogen-containing graphitic materials and catalysts.

Conflicts of interest

There are no conflicts to declare.

Acknowledgements

This work has been financially supported by the MINECO (Spain) project No. CTQ2016-76221-P.

Notes and references

View Article Online
DOI: 10.1039/C9SE00262F

1 Y. Bing, H. Liu, L. Zhang, D. Ghosh and J. Zhang, *Chem. Soc. Rev.*, 2010, **39**, 2184–2202.
2 A. Morozan, B. Jousselme and S. Palacin, *Energy Environ. Sci.*, 2011, **4**, 1238–1254.
3 K. A. Kuttiyiel, K. Sasaki, Y. Choi, D. Su, P. Liu and R. R. Adzic, *Energy Environ. Sci.*, 2012, **5**, 5297–5304.
4 I. E. L. Stephens, A. S. Bondarenko, U. Gronbjerg, J. Rossmeisl and I. Chorkendorff, *Energy Environ. Sci.*, 2012, **5**, 6744–6762.
5 T. Kinumoto, M. Inaba, Y. Nakayama, K. Ogata, R. Umebayashi, A. Tasaka, Y. Iriyama, T. Abe and Z. Ogumi, *J. Power Sources*, 2006, **158**, 1222–1228.
6 V. Briega-Martos, A. Ferre-Vilaplana, A. De La Penìa, J. L. L. Segura, F. Zamora, J. M. M. Feliu and E. Herrero, *ACS Catal.*, 2017, **7**, 1015–1024.
7 K. Gong, F. Du, Z. Xia, M. Durstock and L. Dai, *Science (80-.).*, 2009, **323**, 760–764.
8 L. Qu, Y. Liu, J.-B. Baek and L. Dai, *ACS Nano*, 2010, **4**, 1321–1326.
9 L. Yang, J. Shui, L. Du, Y. Shao, J. Liu, L. Dai and Z. Hu, *Adv. Mater.*, 2019, **31**, 1804799.
10 S. K. Singh, K. Takeyasu and J. Nakamura, *Adv. Mater.*, 2019, **31**, 1804297.
11 X.-K. Kong, C.-L. Chen and Q.-W. Chen, *Chem. Soc. Rev.*, 2014, **43**, 2841–2857.
12 S. Navalon, A. Dhakshinamoorthy, M. Alvaro and H. Garcia, *Chem. Rev.*, 2014, **114**, 6179–6212.
13 L. Dai, Y. Xue, L. Qu, H.-J. Choi and J.-B. Baek, *Chem. Rev. (Washington, DC, United States)*, 2015, **115**, 4823–4892.
14 H. Wang, T. Maiyalagan and X. Wang, *ACS Catal.*, 2012, **2**, 781–794.
15 L. Lai, J. R. Potts, D. Zhan, L. Wang, C. K. Poh, C. Tang, H. Gong, Z. Shen, J. Lin and R. S. Ruoff, *Energy Environ. Sci.*, 2012, **5**, 7936–7942.
16 D. Guo, R. Shibuya, C. Akiba, S. Saji, T. Kondo and J. Nakamura, *Science*, 2016, **351**, 361–5.
17 K. Mamtani, D. Jain, D. Zemlyanov, G. Celik, J. Luthman, G. Renkes, A. C. Co and U. S. Ozkan, *ACS Catal.*, 2016, **6**, 7249–7259.
18 C. V. Rao, C. R. Cabrera and Y. Ishikawa, *J. Phys. Chem. Lett.*, 2010, **1**, 2622–2627.
19 Z.-H. Sheng, L. Shao, J.-J. Chen, W.-J. Bao, F.-B. Wang and X.-H. Xia, *ACS Nano*, 2011, **5**, 4350–4358.
20 T. Xing, Y. Zheng, L. H. Li, B. C. C. Cowie, D. Gunzelmann, S. Z. Qiao, S. Huang and Y. Chen, *ACS Nano*, 2014, **8**, 6856–6862.
21 C. Zhang, R. Hao, H. Liao and Y. Hou, *Nano Energy*, 2013, **2**, 88–97.
22 Y. Feng, F. Li, Z. Hu, X. Luo, L. Zhang, X.-F. Zhou, H.-T. Wang, J.-J. Xu and E. G. Wang, *Phys. Rev. B*, 2012, **85**, 155454.
23 S. Ratso, I. Kruusenberg, M. Käärik, M. Kook, R. Saar, M. Pärs, J. Leis and K. Tammeveski, *Carbon N. Y.*, 2017, **113**, 159–169.
24 Y. Okamoto, *Appl. Surf. Sci.*, 2009, **256**, 335–341.
25 T. Ikeda, M. Boero, S.-F. Huang, K. Terakura, M. Oshima

and J. Ozaki, *J. Phys. Chem. C*, 2008, **112**, 14706–14709.
26 D. Kwak, A. Khetan, S. Noh, H. Pitsch and B. Han, *ChemCatChem*, 2014, **6**, 2662–2670.
27 G.-L. Chai, Z. Hou, D.-J. Shu, T. Ikeda and K. Terakura, *J. Am. Chem. Soc.*, 2014, **136**, 13629–13640.
28 E. F. Holby and P. Zelenay, *Nano Energy*, 2016, **29**, 54–64.
29 I. Matanovic, K. Artyushkova and P. Atanassov, *Curr. Opin. Electrochem.*, 2018, **9**, 137–144.
30 I. Matanovic, K. Artyushkova, M. B. Strand, M. J. Dzara, S. Pylypenko and P. Atanassov, *J. Phys. Chem. C*, 2016, **120**, 29225–29232.
31 N. Wang, B. Lu, L. Li, W. Niu, Z. Tang, X. Kang and S. Chen, *ACS Catal.*, 2018, **8**, 6827–6836.
32 A. Sarapuu, E. Kibena-Põldsepp, M. Borghei and K. Tammeveski, *J. Mater. Chem. A*, 2018, **6**, 776–804.
33 Y. Zhang, J. Ge, L. Wang, D. Wang, F. Ding, X. Tao and W. Chen, *Sci. Rep.*, 2013, **3**, 2771.
34 R. Lv, Q. Li, A. R. Botello-Méndez, T. Hayashi, B. Wang, A. Berkdemir, Q. Hao, A. L. Elías, R. Cruz-Silva, H. R. Gutiérrez, Y. A. Kim, H. Muramatsu, J. Zhu, M. Endo, H. Terrones, J.-C. Charlier, M. Pan and M. Terrones, *Sci. Rep.*, 2012, **2**, 586.
35 A. Ferre-Vilaplana and E. Herrero, *Phys. Chem. Chem. Phys.*, 2015, **17**, 16238–16242.
36 A. Ferre-Vilaplana and E. Herrero, *Electrochim. Acta*, 2016, **204**, 245–254.
37 K. A. Kurak and A. B. Anderson, *J. Phys. Chem. C*, 2009, **113**, 6730–6734.
38 Q. Li, B. W. Noffke, Y. Wang, B. Menezes, D. G. Peters, K. Raghavachari and L. Li, *J. Am. Chem. Soc.*, 2014, **136**, 3358–3361.
39 B. Delley, *J. Chem. Phys. Addit. Inf. J. Chem. Phys. J. Homepage*, 1990, **92**, 508–517.
40 J. P. Perdew, K. Burke, M. Ernzerhof and M. Ernzerhof, *Phys. Rev. Lett.*, 1996, **77**, 3865.
41 B. Delley, *J. Chem. Phys.*, 2000, **113**, 7756–7764.
42 B. Delley, *Mol. Simul.*, 2006, **32**, 117–123.
43 A. Tkatchenko and M. Scheffler, *Phys. Rev. Lett.*, 2009, **102**, 73005.
44 J. Neugebauer and M. Scheffler, *Phys. Rev. B*, 1992, **46**, 16067–16080.
45 J. K. Nørskov, J. Rossmeisl, A. Logadottir, L. Lindqvist, J. R. Kitchin, T. Bligaard and H. Jónsson, *J. Phys. Chem. B*, 2004, **108**, 17886–17892.
46 C. Costentin, M. Robert and J. M. Saveant, *J. Electroanal. Chem.*, 2006, **588**, 197–206.
47 M. T. M. Koper, *Phys. Chem. Chem. Phys.*, 2013, **15**, 1399–1407.
48 C. Hu and L. Dai, *Adv. Mater.*, 2018, 1804672.
49 Y. Jiao, Y. Zheng, M. Jaroniec and S. Z. Qiao, *J. Am. Chem. Soc.*, 2014, **136**, 4394–4403.
50 M. Busch, N. B. Halck, U. I. Kramm, S. Siahrostami, P. Krtil and J. Rossmeisl, *Nano Energy*, 2016, **29**, 126–135.
51 S. Yasuda, L. Yu, J. Kim and K. Murakoshi, *Chem. Commun.*, 2013, **49**, 9627.
52 B. Zheng, X.-L. Cai, Y. Zhou and X.-H. Xia, *ChemElectroChem*, 2016, **3**, 2036–2042.
53 L. Zhao, R. He, K. T. Rim, T. Schiros, K. S. Kim, H. Zhou, C. Gutiérrez, S. P. Chockalingam, C. J. Arguello, L. Pálová, D. Nordlund, M. S. Hybertsen, D. R. Reichman, T. F. Heinz, P. Kim, A. Pinczuk, G. W. Flynn and A. N. Pasupathy, *Science (80-.).*, 2011, **333**, 999–1003.
54 C. H. Choi, H.-K. Lim, M. W. Chung, J. C. Park, H. Shin, H. Kim and S. I. Woo, *J. Am. Chem. Soc.*, 2014, **136**, 9070–9077.
…